Published in final edited form as:
J Chromatogr A. 2009 November 6; 1216(45): 7774–7784. doi:10.1016/j.chroma.2009.09.014.

Protein adsorption and transport in dextran-modified ion-exchange media I. Adsorption

Brian D. Bowes[a], **Harun Koku**[a], **Kirk J. Czymmek**[b], and **Abraham M. Lenhoff**[a]

[a] Department of Chemical Engineering, University of Delaware, Newark, DE 19716, USA

[b] Department of Biological Sciences, University of Delaware, Newark, DE 19716, USA

Abstract

Adsorption behavior is compared on a traditional agarose-based ion-exchange resin and on two dextran-modified resins, using three proteins to examine the effect of protein size. The latter resins typically exhibit higher static capacities at low ionic strengths and electron microscopy provides direct visual evidence supporting the view that the higher static capacities are due to the larger available binding volume afforded by the dextran. However, isocratic retention experiments reveal that the larger proteins can be almost completely excluded from the dextran layer at high ionic strengths, potentially leading to significant losses in static capacity at relevant column loading conditions. Knowledge of resin and protein properties is used to estimate physical limits on the static capacities of the resins in order to provide a meaningful interpretation of the observed static capacities. Results of such estimates are consistent with the expectation that available surface area is limiting for traditional resins. In dextran-modified media, however, the volume of the dextran layer appears to limit adsorption when the protein charge is low relative to the resin charge, but the protein-resin electroneutrality may be limiting when the protein charge is relatively high. Such analyses may prove useful for semiquantitative prediction of maximum static capacities and selection of operating conditions when combined with protein transport information.

Keywords

Protein adsorption; Ion exchange; Dextran-grafted agarose

1. Introduction

Ion-exchange chromatography (IEC) is an important tool in the large-scale purification of proteins. In efforts to improve performance, significant advantages have been realized through the modification of traditional materials with secondary polymers to which functional groups are attached. In particular, several-fold increases in dynamic binding capacity (DBC) have been achieved with such polymer-modified materials, depending on the selected combinations of pH, ionic strength, and flow rate. However, as the DBC is a complex measure reflecting both adsorption and transport properties, further study of the mechanistic basis for such improvements is warranted. In this paper, we focus on how modification with polymers affects the nature and amount of protein adsorption in IEC.

To whom correspondence should be addressed. Tel.: (+1) 302-831-8989; fax: (+1) 302-831-4466; lenhoff@udel.edu.

Some of the first efforts using polymer modification for IEC resins led to “tentacle-type” materials in which linear polyacrylamide chains were end-grafted onto commercially available support matrices [1,2]. One of the major aims of the tentacle structure was to make functional groups more accessible to solute molecules than they would be in a traditional particle [2]. In efforts to characterize “tentacle-type” materials [1–9], significant increases in static binding capacity were observed and were attributed to the ability of protein to adsorb in multilayers rather than in monolayers as in traditional resins. Multilayer adsorption was postulated to arise from Donnan equilibrium behavior [9] as the charges on the protein balanced the opposite, three-dimensionally distributed fixed charges on the resin. An additional advantage of the three-dimensional distribution of functional groups was recognized to be the potential to reduce distortion of the solute upon adsorption [2,10].

Applications of linear end-grafted polymers to other ion-exchange formats such as hollow-fiber membranes [11–15] and monoliths [16,17] may also have influenced the design of currently available resins. For example, a minimum degree of grafting seems to be necessary to achieve the “tentacle-type” binding as the grafted polymers may not protrude into the pore space until they are packed sufficiently closely [16,17], but adsorption capacity increases only to a finite extent with increased grafting density [15].

Subsequent polymer modification efforts have explored options beyond the end-grafting of linear polymers [18]. One example is the HyperD resins [19–23], consisting of a functionalized polyacrylamide gel that entirely fills the pores of a solid support, prompting the “gel in a shell” nickname. This work, on the other hand, focuses on agarose-based materials with dextran extenders. Dextran molecules are branched, relatively bulky, and can potentially be anchored at more than one point in these materials. Therefore, the dextran layer is expected to be less flexible than the linear end-grafted polymers found in materials such as Fractogel, but will still leave more open pore space than in resins such as HyperD that are completely filled by gel.

Agarose-based media with dextran extenders have been examined in a number of studies. For example, Staby and colleagues included the Sepharose XL resins in their efforts to screen a variety of ion exchangers [24,25]. Other studies have looked more mechanistically at factors contributing to the DBC values of proteins on Sepharose XL, requiring some characterization of static capacities [26–30], but were generally more focused on characterization of intraparticle protein transport. Stone and Carta constructed some of their own XL-like particles, examining the effect of the dextran molecular weight on chromatographic performance [31], but were again focused more on transport behavior.

In this work, protein adsorption is characterized on the traditional SP Sepharose Fast Flow (SP Sepharose FF or SP FF) resin and on the dextran-modified resins SP Sepharose XL (SP XL) and Capto S. As in other studies, one aspect of this work is to examine adsorption isotherms under a variety of solution conditions. While some studies focus only on small model proteins or on the large antibodies that are increasingly produced as therapeutics, this study examines the role that protein size might play in adsorption by using proteins of a range of sizes. Additionally, a significant aspect of this work is to use knowledge of resin and protein properties to rationalize how observed adsorption capacities might be related to the physical limits of the resins.

2. Materials and methods

2.1. Buffers and protein samples

Monobasic sodium phosphate (NaH_2PO_4) was purchased from Fisher Scientific (Fair Lawn, NJ) and used to prepare pH 7 solutions. At this pH, total ionic strength (TIS) values of 2, 6, and 20 mM were achieved using 1, 3, and 10 mM sodium phosphate, respectively, and ionic

strengths of 50 and 100 mM were reached using 10 mM sodium phosphate with appropriate amounts of sodium chloride (Fisher Scientific). Acetic acid was purchased from Mallinckrodt Chemicals (Phillipsburg, NJ) and formic acid was purchased from Acros Organics (Geel, Belgium). Solutions at pH 5 and pH 3 were prepared using 10 mM acetic acid and 10 mM formic acid, respectively, with sodium chloride added as necessary to adjust ionic strength. All buffers were filtered at 0.22 μm prior to use.

Hen egg white lysozyme was purchased from Sigma-Aldrich (St. Louis, MO). Bovine lactoferrin was generously donated by DMV-International (Veghel, The Netherlands). A monoclonal antibody (mAb) was generously donated by Biogen Idec (San Diego, CA). Both the lysozyme and lactoferrin solutions were prepared by first dissolving the protein into buffer, while the mAb was provided in a concentrated solution. Lactoferrin required initial purification, which was achieved using a sodium chloride gradient in pH 7, 10 mM phosphate buffer on a 28 cm × 1.6 cm i.d. SP Sepharose XL cation-exchange column. Final protein solutions were prepared by using either 5 or 50 kDa Amicon Ultra4 centrifugal filters from Millipore (Billerica, MA) to concentrate a sample, rediluting with fresh buffer, and repeating two additional times to ensure the correct buffer composition in the protein samples prior to use. Due to the Donnan effect, which can cause differences in pH between the retentate and permeate because of unequal distributions of ions, some titration with higher pH buffer was needed to reach the correct pH when preparing samples with less than 10 mM buffer. Protein solutions were filtered at 0.22 μm and concentrations were determined using UV spectrophotometry (UV-1700, Shimadzu, Kyoto, Japan) with extinction coefficients at 280 nm of 2.64, 1.51, and 1.61 cm^2/mg for lysozyme [32], lactoferrin [33], and the mAb [34], respectively. Protein characteristics used in the interpretation of adsorption behavior are included in Table 1.

2.2. Stationary phases

The traditional resin SP Sepharose Fast Flow and the dextran-modified resins SP Sepharose XL and Capto S, all strong cation exchangers, were obtained from GE Healthcare (Piscataway, NJ). Key resin properties are summarized in Table 2. These three resins may be referred to simply as FF, XL, and Capto, respectively, when it is the base matrix itself, regardless of the ion-exchange moiety, that is of interest. SP FF consists of an agarose base matrix derivatized with a sulfonate group on a six-carbon spacer arm [35]. SP XL uses the same agarose base as SP FF, but 40 kDa dextran (A. Axén, personal communication) is grafted onto the agarose prior to functionalization such that both the agarose backbone and the dextran can carry functional groups; the process can result in attachment of each dextran molecule at more than one point [31]. The use of the same base material in SP FF and SP XL is advantageous for making direct chromatographic comparisons. Capto S is prepared in a similar manner to SP XL, using a similar amount of 40 kDa dextran, but a different crosslinking method is used on the agarose, making the particles more rigid, thereby allowing operation at higher flow rates (A. Axén, personal communication). Additionally, the manufacturer notes that the sulfonate group is attached via a shorter spacer arm, residing on an ethyl group instead of the six-carbon spacer arm found in SP FF and SP XL.

2.3. Capillary tube calibration

The hydrated particle volume, being the volume of the spherical particles themselves in aqueous solution, was selected as a convenient measure of the amount of resin being used as it provides a basis for normalization of properties such as adsorbed protein amounts, independent of particle packing. The procedure for determining the hydrated particle volume employs blue dextran, which is fully excluded from the pores of the particles, and is based on comparisons of the elution volumes of injections performed on an empty column and one packed with particles.

Injections were performed on a Waters 2695 chromatography workstation (Waters Corporation, Milford, MA) using a Waters 2996 photodiode array detector to observe blue dextran absorbance at 280 nm. All injections were performed in triplicate on a 0.5 cm i.d. column and consisted of 10 μL of 1 mg/mL blue dextran in DI water run at 0.05 mL/min. This low flow rate was selected to limit compression of the particles. Retention volumes were determined based on the first moment of the elution profiles. Injections were first run for the column with the two flow adaptors directly in contact to determine the volume of tubing between the injection point and the photodiode array, V_d. To dose particles to the column, a slurry of particles in DI water was first allowed to gravity settle in Wiretrol II 100 and 200 μL capillary tubes (Drummond Scientific Company, Broomall, PA). The settled height of particles was measured and the particles were added to the column where they were again gravity settled. The top flow adaptor of the column was adjusted to touch the top of the settled particle bed without compression and then new injections were run. The hydrated particle volume, V_{hyd}, was calculated as

$$V_{hyd}=V_c-(V_R-V_d) \tag{1}$$

where V_c is the total column volume determined by multiplying the cross-sectional area by the measured distance between the flow adaptors and V_R is the retention volume of blue dextran in a packed column. The quantity in parentheses is the interparticle void volume of the column. A resin-specific calibration factor was determined by dividing the hydrated particle volume by the settled capillary tube height, allowing for accurate dosing of particles with the capillary tubes in subsequent experiments.

The calibration factors for the three resins were found to be quite similar, which is not surprising given the similar particle sizes provided by the manufacturer. The values correspond to interparticle void fractions of 0.42, 0.38, and 0.40 for FF, XL, and Capto, respectively, which are similar to those expected for the random packing of spheres gravity settling from a slurry [36].

2.4. Adsorption isotherms

To measure adsorption isotherms, particles were packed into a small column and washed with at least twenty column volumes each of DI water, 1 M NaCl, and again DI water, and then were equilibrated in the desired buffer solution using at least twenty column volumes. The particles were collected and then Wiretrol II 100 and 200 μL capillary tubes were used to add known volumes of the equilibrated particles to Eppendorf tubes containing known amounts of protein in a buffer of the same composition. Solutions were rotated slowly for at least 24 hours and sometimes for several days as needed to confirm that no additional uptake occurred. After equilibration, the Eppendorf tubes were spun down and the protein concentration in the supernatant, C, was measured. The adsorbed protein concentration, q, which includes unadsorbed protein within the pores of the particles, was determined from a mass balance. Care was taken to account for the small volume of liquid in the capillary tubes that was added to protein samples in the process of adding particles, as this extra volume affects the values of the liquid volume and the initial protein concentration. Unless stated otherwise, all adsorbed concentrations refer to the mass of protein per hydrated particle volume.

2.5. Electron microscopy imaging

Both transmission and scanning electron microscopy were employed to examine the differences in protein adsorption and localization in the traditional and dextran-modified media. These studies focused on FF and XL, as the comparison of these resins most directly

probes the effect of the dextran. The Q versions of these resins were studied here, but limited imaging of the SP versions (not included) confirmed that the results are qualitatively similar.

2.5.1. Transmission electron microscopy (TEM) imaging—To prepare the resins for imaging, 200–800 μL settled volume of Q Sepharose Fast Flow (Q FF) or Q Sepharose XL (Q XL) was measured using Wiretrol II 100 and 200 μL capillary tubes. The resin samples were then added to 15 mL of 5 mg/mL α-lactalbumin (Sigma, purity 85%) in a 20 mM phosphate buffer solution at pH 8. The samples were left rotating in conical tubes overnight (12–14 hours) to equilibrate. The amount of protein uptake was calculated by mass balance using the supernatant concentration determined by the absorbance at 280 nm with an extinction coefficient of 2.01 cm^2/mg [37].

All chemicals used for fixing, embedding, and staining the samples were obtained from Electron Microscopy Sciences (Hatfield, PA). Standard protocols [38] employed in the preparation of biological specimens for TEM imaging were followed. Resin samples were first chemically fixed by 1% paraformaldehyde and 1% glutaraldehyde in a 50 mM phosphate buffer solution, embedded in 3% agarose and cut into 1–2 mm thick strips, and then fixed with 2% osmium tetroxide for 1–2 hours. Following dehydration in a graded series of glass-distilled acetone, the samples were infiltrated with the Embed-812 resin kit mixture and cured for 72 hours in a 65°C oven. Sample blocks were faced and approximately 65 nm thick sections were obtained with a diamond knife (DDK, Wilmington, Delaware) using a Reichert-Jung Ultracut E microtome. These sections were placed on 200 mesh formvar-carbon supported copper grids and post-stained with Reynolds lead citrate and methanolic 2% uranyl acetate solutions. Digital images were acquired with a Mega View II camera (Olympus, Münster, Germany) on a Zeiss CEM 902 TEM operated at a voltage of 80 kV.

2.5.2. Scanning electron microscopy (SEM) imaging

Samples of Q FF or Q XL with adsorbed protein were prepared and chemically fixed as described above. After fixation, the samples were dehydrated in a graded series of ethanol, placed in 30 μm microporous specimen capsules (Electron Microscopy Sciences) and CO_2 critical point dried (Tousimis, Autosamdri-815B, Series A). Dry samples were mounted on aluminum stubs using double-sided sticky carbon tabs. The periphery of each sample was coated with a thin layer of silver conductive adhesive paint (type 503, Electron Microscopy Sciences) to enhance conductivity. The samples were then palladium-gold sputter-coated using a Denton Bench Top Turbo III coater for 2.3 minutes at a current of 30 mA and an argon pressure of 65 mtorr. Imaging of the samples was carried out using a Hitachi S4700 FESEM operated in the secondary electron mode with a voltage of 3.0 kV and a working distance of 3–4 mm.

2.6. Isocratic retention

Isocratic retention experiments were performed in pH 7, 10 mM phosphate buffer (lysozyme and lactoferrin) or pH 5, 10 mM acetate buffer (mAb) with sodium chloride added to adjust the TIS. The highest TIS values used, namely 1.02 M for lysozyme, 1.52 M for lactoferrin, and 0.7 M for the mAb, were found to be sufficiently high to prevent protein retention. A target k value on the order of 100 was used to determine the lowest ionic strengths used.

Experiments were run on the same Waters system as used in the capillary tube calibrations, again with detection by absorbance at 280 nm. Protein solutions were prepared at the same ionic strengths at which they were to be isocratically injected and eluted. Protein concentrations ranged from roughly 0.5 mg/mL for the highest ionic strengths, where protein was unretained, to roughly 5 mg/mL for the most strongly retained samples, as higher concentrations were needed to ensure that the absorbance signals would be strong enough given the broad peaks.

Technically, to measure *k*, concentrations need to remain low enough for adsorption to be in the linear portion of the isotherm, which may not have held for the lowest ionic strength samples. However, no concentration effects were discernible, so it is likely that, if there was any deviation from linearity, samples traveled a negligible distance in the column before becoming dilute enough to return to the linear portion of the isotherm. Samples consisted of 20 μL injections onto HiTrap 1 mL columns (2.5 cm × 0.7 cm i.d.) run at 0.2 mL/min (≈31 cm/hr). The first moments of the peaks were used to determine retention times, although the peak maxima could probably have been used with little error since peaks were generally Gaussian in appearance. The retention factor, *k*, was calculated using

$$k = \frac{t_R - t_{HS}}{t_{HS} - t_d} \tag{2}$$

where t_R is the retention time of a sample run at the ionic strength of interest, t_{HS} is the retention time of the unretained high-salt sample, and t_d is the system dead time as determined by an injection without the column in place.

3. Results and discussion

3.1. Adsorption isotherms

The focus in this section is on characterization of adsorption behavior, especially in terms of static capacity (from estimates of isotherm plateau values) and response to changes in ionic strength. In subsequent sections, properties of the proteins and resins are used to rationalize the observed behavior. Adsorption isotherms were measured for each protein-resin pairing at TIS values that were selected based on ranges of interest found in frontal loading experiments (not shown). The isotherms are shown in Figure 1, with Langmuir isotherm fits to guide the eye and with all plots on the same axes to aid direct comparisons.

The top row of Figure 1 shows the isotherms for lysozyme on the three resins. The data for lysozyme adsorption on SP FF have been adapted from those of Dziennik et al. [39,40] by correcting for the SP FF calibration factor determined in this work. All curves reflect typical behavior of decreasing static capacity and rectangularity with increasing ionic strength. However, there are differences in the magnitudes of the responses of the resins to increases in ionic strength. For example, for the dextran-modified resins, there is only a small decrease in static capacity between 2 and 20 mM ionic strength, while the same increase in salt for SP FF results in roughly a 30% drop in static capacity. In examining the magnitudes of the static capacities, it is clear from the 2 mM data, for example, that the two dextran-modified resins have higher static capacities than SP FF. SP XL does exhibit a small capacity advantage over Capto S.

The lactoferrin adsorption data are shown in the middle row of Figure 1. Uptake was found to be quite slow for this protein, especially for the lowest ionic strength on SP FF. As such, the lowest protein concentration points may not have been fully equilibrated, making the low-salt isotherms appear less rectangular than they truly are. This limitation is probably why the 100 mM isotherm on SP FF appears more rectangular than the 50 and 20 mM curves, for example. Therefore, some care must be made in examining the lactoferrin isotherms, but this concern is important only for solution concentrations of a few tenths of a mg/mL or less, meaning there would be limited value in repeating the experiments.

At higher lactoferrin concentrations, interestingly, all three resins have about the same static capacity at the lowest tested ionic strength of 20 mM. The fact that SP XL and Capto S have

similar capacities at this low salt concentration is not surprising given the similar lysozyme behavior. Capto now has the higher capacity of the dextran-modified resins, but the XL capacity may reach that of Capto at an even lower ionic strength given the greater increase in XL capacity between 50 mM and 20 mM.

While the subtle reversal in which dextran-modified resin has the higher capacity is of note, there are two more significant changes in behavior in comparing lysozyme and lactoferrin adsorption. First, in contrast to the behavior for lysozyme, the static capacity for lactoferrin drops more significantly for increases in ionic strength on the dextran-modified materials than for SP FF. This is especially noticeable at 200 mM TIS, where the SP FF capacity is roughly double those of SP XL and Capto S. The other significant difference from lysozyme behavior is, as was previously noted, the fact that the SP FF capacity at low ionic strength is now high enough to be comparable to those of SP XL and Capto S. To understand this behavior, it is helpful to consider the charge distribution of lactoferrin, which is shown in Figure 2. Unlike lysozyme, which is globular with a relatively uniform charge distribution [41], lactoferrin is roughly dumbbell shaped, with one very positively charged patch on the side of one of the lobes. The high charge likely gives a dominant binding orientation with this patch in contact with the resin surface, perhaps causing the protein to bind with its longest dimension nearly perpendicular to the resin surface. Since the rest of the protein is relatively neutral, the molecules may also be able to pack closely together. This combination of tight packing and a relatively small footprint on the resin surface could give rise to an anamolously high static capacity on SP FF.

Isotherms for the mAb (bottom row of Figure 1) are more similar to the lysozyme isotherms than the lactoferrin ones in that the dextran-modified media again have a clear static capacity advantage over SP FF at the lowest ionic strength, with the SP FF capacity being only about half those of the other two resins. The low capacity suggests that the accessible surface area of SP FF is insufficient to allow adsorption on par with that in the dextran-modified media. In comparing the ionic strength effects, there are fairly significant differences in the behavior of the two dextran-modified media. While SP XL and Capto S have roughly the same static capacity at 6 mM TIS, the capacity of SP XL clearly drops more rapidly with increasing ionic strength than for Capto S, to the point that the 100 mM curve for SP XL is a bit lower even than that for SP FF.

3.2. Electron microscopy

TEM images were taken for both low (Figure 3) and high (Figure 4) adsorbed protein concentrations. The darker areas correspond to the stained protein and the lighter areas correspond to the void space.

For low protein loading in FF (Figure 3a), the protein seems to bind only on the surface of the agarose fibers, which is expected based on the resin properties. For XL (Figure 3b), some binding along the agarose surface seems to be present too, but there are also large dark patches, suggesting that a significant amount of protein partitions into the dextran layer as well.

At high protein loading, the binding on FF (Figure 4a) is qualitatively similar to that at low protein loading. Again, this behavior is consistent with the localization of the FF functional groups on the agarose surface, so the higher amount of adsorbed protein appears to correspond simply to a higher surface coverage. For XL (Figure 4b), almost all resemblance to FF is lost at the high protein loading. The primary features are the large patches of protein, which may be interpreted as the dextran layer being swollen with protein. Therefore, it seems that a significant reason for the increased static binding capacities of the dextran-modified media at low salt, as compared to those of FF, is that the dextran layer allows protein to occupy a larger volume fraction of the particle.

To provide a three-dimensional view of the differences in protein adsorption on the two resins, they were also viewed at high protein loading conditions using SEM (Figure 5). As was the case for TEM, the images for FF (Figure 5a) seem to reflect binding of protein only along the agarose fiber surfaces, while the images for XL (Figure 5b) suggest that a significant amount of protein has partitioned into the dextran layer. Comparison of these SEM images for high protein loading in FF and XL also makes it clearer than in TEM that a significantly larger volume fraction is occupied by protein in XL than in FF. Although some of the filled volume in the SEM images may be due to the palladium-gold coating, examining the SEM images in concert with the TEM images, where this coating was not employed, shows that it is the difference in bound protein that is primarily responsible for the observed differences between FF and XL.

3.3. Isocratic retention

Results of the isocratic retention experiments are shown in Figure 6, with earlier data for lysozyme on SP FF [42] included for comparison. The data, showing k as a function of total ionic strength in log-log form, are roughly linear, qualitatively consistent with the stoichiometric displacement model [43], although plotting log k as a function of $1/\sqrt{\text{TIS}}$ [44] also gives a roughly linear trend. In addition to the k values in Figure 6, retention times are shown for protein-resin pairings for which k values could not be appropriately defined. These cases are addressed in the section following this one.

One striking feature in Figure 6 is that the curves for lysozyme on the three resins at pH 7 are very similar, suggesting that the retention mechanism of lysozyme is quite similar in these resins. The similarity might result from the use of the same functional group in these resins, despite the difference in distribution of these groups in the traditional and dextran-modified materials and despite the shorter spacer arm used in Capto. The similarity is also interesting given that retention was found to increase with decreasing spacer arm length for SP FF variants, but that increase may have been due to increased nonelectrostatic interactions with the base matrix for shorter spacer arms [45], which would not be expected to happen here.

The slope of the linear portion of an adsorption isotherm is indicative of adsorption strength and is proportional to k. Thus, the k data for the mAb on SP FF show that significant changes in adsorption strength occur over a fairly low and narrow ionic strength range at the chosen pH of 5. Since steeper initial isotherm slopes not only indicate stronger adsorption, but also typically correspond to higher static capacities [46], the rapid changes in k over this low ionic strength range are consistent with the larger drop in the SP FF static capacity for the mAb than for lysozyme in going from 6 mM to 100 mM TIS (Figure 1). The curve for lactoferrin on SP FF reflects significant retention, even at high ionic strengths. This behavior may be due to the presence of the previously noted (Figure 2) highly charged patch on one lobe of the protein such that relatively high salt concentrations would be needed to screen the electrostatic attraction between that patch and the oppositely charged resin effectively. The retention behavior of lactoferrin on SP FF is consistent with the relatively high static capacity of SP FF even up to 200 mM TIS.

3.4. Exclusion of larger proteins from dextran layer

Retention factors for lactoferrin and the mAb on the two dextran-modified resins are not shown in the previous section because these larger two proteins are almost completely excluded from the dextran layer at high ionic strengths, as evidenced by their early elution. Rather, to give some sense of the behavior, retention times are shown in Figure 6, where available. Steric hindrance is expected to be at play in this exclusion, as has been suggested for the exclusion of macromolecules from polyacrylamide gels [47] such as those found in HyperD [19]. However, there may also be an electrostatic contribution. For example, neutral dextran probes

of roughly the same size as the mAb can access a much smaller fraction of the pore volume for Capto than for XL [48] (B. To, personal communication), but at high salt, the mAb itself can access similar fractions of the pore volumes in the two resins. Regardless of the cause, the exclusion at high salt confounds the definition of *k* for these protein-resin pairings since changes in ionic strength result in changes not only in adsorption strength, but also in accessible volume.

Comparing the retention times for the mAb on XL and Capto with the *k* values for the mAb on FF shows that all the data follow roughly the same trend. This result is consistent with the similarity of the data for lysozyme on all three resins and is indicative of the fact that the exclusion behavior does not significantly affect retention at the low ionic strength range of interest for the mAb at this pH. For lactoferrin on XL, on the other hand, the slope of the retention time data deviates noticeably from that of the *k* values for lactoferrin on FF. The deviation probably arises because the data are at high ionic strengths where exclusion of lactoferrin from the dextran layer of XL is expected to be significant.

More significant than the difficulty in defining *k* values is that the exclusion is likely the cause of the suppressed static capacities for lactoferrin on XL and Capto at 200 mM TIS or for the mAb on XL at 100 mM TIS. It should be stressed that the high-salt exclusion behavior encountered here is entirely different from the low-salt electrostatic exclusion mechanism proposed by Dziennik et al. [49] and Harinarayan et al. [50]. The latter exclusion behavior is a kinetic effect thought to occur when protein molecules adsorbed on the pore surface repel other protein molecules that are entering the pore, thereby slowing uptake under conditions where the static capacity will be high. The exclusion at higher salt here, on the other hand, seems to be a thermodynamic effect.

Intriguingly, in polymer-modified media with linearly-grafted polymers such as Fractogel, the polymers seem to collapse at high salt when the charges on the polymers are well screened, opening the pore space [51] and reducing the binding volume. The dextran in XL and Capto is branched and is of higher molecular weight than the polymer used in Fractogel, so, combined with its potential for attachment at more than one point, the dextran would not be expected to collapse as easily as the polymer in Fractogel. Experimentally, the inability of larger, less flexible polymer extenders to collapse at high salt has been observed for Super Q-650C [52], for example. Therefore, the exclusion behavior in XL and Capto causes a loss in capacity, in spite of a relatively constant binding volume. Thus, media modified with short, collapsible polymers or with large, comparatively immobile polymers can both suffer significant losses in static capacity with increasing salt, even though the mechanism of loss is different.

3.5. Relation of resin and protein properties to adsorption properties

Trends such as those observed in the adsorption isotherms in this work can play a significant role in the optimization of separations, so it is desirable to determine how they are controlled by the properties of the selected resins and proteins. An effort to do this is undertaken here, with the emphasis on estimating physical limitations on adsorption capacity in order to put observed adsorption amounts in context. As such, both available space and available charge of the resins are considered, as these are two of the most obvious determinants of adsorption.

Using phase ratio and charge density data for traditional media, such as FF, it can be estimated that proteins bind in proximity to multiple resin surface charges, as is considered in the steric mass action (SMA) formalism [53]. Thus, under most conditions, the resin charges are too tightly packed for adsorption to be controlled by available resin charges, suggesting that available surface area for binding will be limiting. If protein molecules are approximated as spheres, the jamming fraction of roughly 0.547 in random sequential adsorption (RSA) [54–57] and the hexagonal packing fraction of $\pi/(2\sqrt{3}) \approx 0.907$ set reasonable lower and upper

bounds, respectively, for the fraction of the surface area that can be occupied by protein. Such estimated ranges for lysozyme and bovine serum albumin come reasonably close to capturing experimental adsorption capacities on traditional media [52]. Estimated ranges for lactoferrin and the mAb on SP FF, likewise, give reasonable agreement with the experimental values found in this work. Discrepancies may be due to a number of factors, including sensitivity to the estimates of the available surface area and the protein radius or neglect of the effects of protein-protein repulsion and protein orientation.

For polymer-modified resins such as XL and Capto, it is not immediately apparent whether available resin charge or available binding space will limit adsorption. Also, it is clear that available surface area is not an appropriate measure of binding space for these resins as use of this area can lead to severe underestimates of static capacity [52]. Instead, the available volume for adsorption has been suggested as a more reasonable description of the binding space [18], consistent with what is suggested by the TEM images (Figure 4) in this work. For media, such as HyperD, that have pores entirely filled with gel, the binding volume should be simple to estimate, but the task is less simple for media like XL that have incompletely-filled pores. Thus, the analysis starts with an estimate of the binding volume in XL.

3.5.1. Dextran volume—While the TEM images (Figure 4) could perhaps be used to estimate the dextran volume fractions, there is always some danger in using localized properties to infer global ones or in using two-dimensional projections to study three-dimensional features. Instead, a more indirect approach is taken to estimate the average thickness of the dextran layer using inverse size-exclusion chromatography (ISEC) to estimate the pore size distributions of resins. Differences in the ISEC distribution coefficient, K_d, for FF and XL should reflect the pore volume that is occupied by the grafted dextran in XL. ISEC results are available for Q FF and Q XL with glucose used as the smallest probe and dextran of various molecular weights as the larger probes [52]; these results are reproduced in Figure 7. Information available from the manufacturer suggests that the identity of the functional group is the only significant difference between the Q and SP versions of these resins, so it is expected that results would be similar for the SP versions.

The fraction of the particle accessible to the smallest probe, glucose, which defines the intraparticle porosity, ε_p, was found to be 0.79 for both Q FF and Q XL and was also used to define a K_d value of unity [52]. Given that the intraparticle porosities of FF and XL are about the same, if there exists a probe that is completely excluded from the dextran layer, one can associate differences in K_d values for this probe on the two particles with the fraction of the pore volume that is occupied by the grafted dextran layer. It is apparent that the smallest probes can penetrate into the dextran layer in XL since the glucose-determined porosity is the same as for FF and since the K_d values for the smallest dextran probes are quite similar to those for FF. However, it is also apparent that the larger probes are increasingly excluded from the dextran layer as the K_d values for XL become significantly smaller than for FF. While larger probes are more clearly excluded from the dextran layer, they are also increasingly excluded from FF, so obtaining a definitive measure of the dextran volume is problematic. With this concern in mind, the dextran probe with a 3.89 nm viscosity radius was assumed to be completely excluded from the dextran layer because this probe had a small, positive $K_{d,XL}$ value and gave the largest experimental value of $K_{d,FF} - K_{d,XL}$, namely 0.59.

To describe the pores of XL, a model accounting for the thickness of the dextran layer can be employed. From the electron microscopy results in this work, it seems clear that the dextran layer is heterogeneous. However, since it is really the volume of the dextran layer that is sought, an estimate of the average thickness of the dextran layer will suffice.

In a simple approximation, resin pores can be modeled as being cylinders of a single radius, such that K_d is the fraction of the pore cross-sectional area accessible to the center of a spherical probe of radius r_{probe}:

$$K_d = \frac{(R_{lumen} - r_{probe})^2}{R_{pore}^2} \tag{3}$$

where R_{pore} is the entire pore radius and R_{lumen} is the radius of the open pore space. For a FF-type pore, shown in Figure 8a, $R_{lumen} = R_{pore}$. A nonlinear fit of theoretical FF K_d values to the experimental ones yields an estimate of R_{pore}=24.9 nm. For an XL-type pore (Figure 8b), an impenetrable dextran layer of uniform thickness, r_{dex}, coating the pore wall is considered, such that $R_{lumen} = R_{pore} - r_{dex}$. By matching the experimental and theoretical values of $K_{d,FF} - K_{d,XL}$, a value of r_{dex}=12.2 nm was estimated based on the K_d values of the dextran probe with a 3.89 nm viscosity radius. Therefore, based on evaluation of $K_{d,FF} - K_{d,XL}$ for a probe of zero radius, the fraction of the pore volume occupied by the dextran layer was estimated to be 0.74. Application of this analysis to limited data available for the SP versions of FF [51] and XL [48] (B. To, personal communication) yields an estimated dextran-occupied fraction of 0.78. This value is similar to that for Q XL, in spite of potential uncertainties due to the SP data originating in separate studies. The similar results give some confidence that, as expected from knowledge of the resin properties, the identity of functional group is not an important factor and that the results for the Q versions of the resins are applicable to the SP versions.

As a more physically realistic model of agarose materials, we can instead consider the theoretical value of K_d based on the calculations of Ogston for the space accessible to a spherical particle in a suspension of randomly oriented rods [58]. The K_d value for the Ogston model is given by [59]

$$K_d = \frac{1}{\varepsilon_p} \exp\left[-\pi L (r_{probe} + r_{rod})^2\right] \tag{4}$$

where L is the concentration of rods in terms of length per volume and r_{rod} is the radius of the rod. A nonlinear fit of the K_d data for FF gives values of $L = 1.23 \cdot 10^{15}$ m/m^3 and r_{rod}= 8.15 nm. For XL, the rod thickness in Equation 4 effectively increases by r_{dex}. Fits for this model yield r_{dex} = 12.0 nm and a dextran-occupied fraction of 0.72, which are quite similar to the values found from the cylindrical pore model, giving some confidence that the estimates are reasonable. Comparison of these values with estimates obtained from polymer physics theory of terminally-anchored polymers (for example, [60]) suggest that a 12 nm thickness is reasonable, but such estimates are rather imprecise due to inconsistent estimates of characteristic length scales of dextran in the literature (see for example, [61] for discussion) and the approximate nature of the theory. Depending on protein size, the estimated 12 nm thickness of the dextran layer in XL would be sufficient for two to four layers of protein to reside within the dextran, offering ample space for more adsorption than would be possible for the anticipated monolayer coverage of protein on the agarose surface of FF.

Unfortunately, the procedure used here to estimate the dextran volume of XL cannot be applied to Capto. This is because there is no commercially available media with the same base matrix as Capto, but without dextran modification, which would serve the comparative role that FF did for XL. Therefore, Capto is not explicitly treated here, but as a first approximation we could assume that Capto and XL afford similar binding volumes.

3.5.2. Spatial limitations on adsorption—Estimates of intraparticle porosities are 0.79 [52] and 0.84 [51] for the Q and SP versions of FF, respectively, so the estimate that the dextran layer occupies 72–74% of the FF pore volume suggests that roughly 60% of the XL particle volume is available for binding. If the proteins are approximated as spheres, the most dense packings of face-centered cubic (fcc) or hexagonal close-packed (hcp) give occupied volume fractions of $\pi/(3\sqrt{2}) \approx 0.74$. Combining this packing fraction with a partial specific volume of about 0.7 cm^3/g typical of most proteins (see Table 1) leads to an estimate that XL affords the volume for roughly 630 mg of protein per mL of hydrated particle volume. However, this estimate is much higher than experimental values and uses no protein-specific information. As a refinement, the hydrodynamic radius can be used instead of the radius of a sphere of equivalent volume, as the former should more realistically account for protein solvation and shape. Using hydrodynamic radii of 2.01 nm [62], 3.33 nm [63], and 4.5 nm [64] for lysozyme, lactoferrin, and monoclonal antibodies, respectively, the respective estimates are reduced to 320, 390, and 290 mg/mL. Some uncertainty in the estimates arises from not considering the volume occupied by the dextran itself or the actual packing of the aspherical protein molecules, but values should still prove useful in interpreting the observed binding.

At low salt, experimental XL capacities for lysozyme and the mAb are roughly 340 and 330 mg/mL, respectively, and, as is discussed in the following section, lactoferrin adsorption on SP XL at pH 5 reaches roughly 400 mg/mL. Thus, despite the approximate nature of the analysis, the spatial-limit estimates obtained using the hydrodynamic protein radii are within 15% of the maximum experimental static capacities, giving some confidence that this approach could be used to predict maximum static capacities for other proteins and that available volume is a reasonable determinant of static capacity in XL. It is not surprising that the estimates are better for XL than for FF as protein orientation should have less of an effect on protein packing densities for a fixed volume than for a fixed surface area.

3.5.3. Charge limitations on adsorption—Another factor that can limit static capacity is that of electroneutrality in the protein-resin systems, that is, to assume that the static capacity is determined by how much protein would balance the charge on the resin. Since we do not have any sequence or titration information for the mAb, the analysis here is limited to lysozyme and lactoferrin, for which net charge as a function of pH is available from experiment or calculation. For lysozyme, such information is taken from experimental data at 0.1 M ionic strength [65]. For lactoferrin, net charge information was estimated using the PDB2PQR program [66], which employs PropKa [67] to estimate the pK_a values of the residues. The net charge versus pH data are summarized in Table 3. In considering the charge on the resins, the ranges of charge densities provided by the manufacturer were used (Table 2). Resulting static capacity estimates are included in Table 3. As was alluded to previously, such calculations are expected to overestimate capacity for FF, but the estimates could be more reasonable for XL and Capto, in which charges are distributed in three dimensions.

To aid in the interpretation of the charge-based static capacity estimates, additional isotherm data probing the effect of pH were collected, all at 20 mM TIS, and are included in Figure 9. The shapes of these isotherms are not all suitable for Langmuir isotherm fits, so no visual fits are provided. These isotherms are all on the same axes for comparison, but the scales are different from those used for the isotherms showing the ionic strength effect.

The pH effect isotherms obtained for lysozyme are shown in the top row of Figure 9. For SP XL and Capto S, the static capacity falls with increasing net charge (decreasing pH). For SP FF, though, the static capacity is nearly constant over the pH range studied, possibly due to a balance between increased protein-surface attraction and increased protein-protein repulsion with increasing net protein charge. Comparison of the lysozyme-FF capacities, which have values of roughly 180–210 mg/mL, with the charge-limited capacity estimates in Table 3 shows

that the experimental capacities are significantly lower than the estimated ones, again consistent with available surface area being the limiting factor.

For XL and Capto, the distribution of charge between the agarose backbone and the dextran extenders is unknown, so, while the total resin charge is known, the spacing of charges is not. For XL, the charge-limit estimates are much higher than the experimental values while the spatial-limit estimates are quite close. This finding suggests that protein reaches it spatial-limit before enough protein can be adsorbed to neutralize the resin charges. For Capto, on the other hand, the experimental capacities are on par with those estimated based on the lower end of the charge density range and it may be that experimental capacities at lower ionic strengths would better match the charge-limited estimates. It seems that lysozyme alone can roughly neutralize all of the resin charges and that resin charge rather than available volume will limit adsorption. Essentially, this suggests that the sparser spacing of charges in Capto may allow it to take greater advantage of its functional groups than is possible in FF and XL. Interestingly, Dismer et al. found evidence for a preferred multi-point interaction between lysozyme and SP XL [68], but is unclear what effect the different spacing of charges in Capto might have on such interactions.

The pH effect isotherms for lactoferrin are in bottom row Figure 9. One of the most striking features of these plots is that, at the lowest pH of 3, the isotherm for each resin seems to increase roughly linearly with protein concentration, but with an apparent non-zero vertical intercept. While stability was not assessed in this work, previous studies suggest that lactoferrin is stable at this pH [69], so it is not expected that a non-native state is the cause of this behavior. The observed isotherm shape likely means that there is strong protein-surface attraction, giving a steep isotherm slope for solution concentrations up to roughly 0.1 mg/mL, where protein-protein repulsion should be minimal. Above this concentration, though, strong protein-protein repulsion may significantly limit adsorption, accounting for the modest increases in adsorption with increased protein concentration. Perhaps with the exception of the SP FF curve, the pH 3 adsorption capacities do not even appear to plateau over the studied range of protein concentrations. The experimental capacities for XL and Capto do approach the lower charge-limited estimates at this pH, but the lack of isotherm plateaus makes it hard to compare the experimental and estimated capacities meaningfully.

At higher pH values, the charge-limited estimates are well above both the spatial-limit estimates and the experimental capacities. At pH 5, as was previously mentioned, the XL capacity does seem to be in agreement with the spatial-limit estimate based on the hydrodynamic radius of lactoferrin. Since the dextran volume for Capto could not be estimated in the way it was for XL, it is not known whether lactoferrin is already binding near its spatial limit at pH 7, which would account for why the capacity does not increase for pH 5 the way it does for XL. In any case, as would be expected to be true especially at pH 3, protein-protein repulsion could prevent protein adsorption from reaching charge- or spatially-limited static capacity estimates, complicating this simple analysis.

4. Conclusions

This work showed that the higher capacities observed in the isotherms for dextranmodified media at low salt may be achievable simply because the dextran affords a larger protein binding volume. However, isocratic retention experiments showed that larger proteins can be almost completely excluded from the dextran layers of these resins at high salt. This exclusion behavior could have important consequences in resin selection for purification processes in which low-salt conditions are undesirable or unaffordable.

Studies often present adsorption isotherms for a variety of solution conditions, but usually only relative static capacity comparisons can be made as there is no consideration of the physical limits of the resins. This work showed the value of using basic information about the structure and charge of the proteins and resins to rationalize observed binding behavior. For traditional resins, such as FF, available surface area seems to be the factor limiting how much protein can adsorb. For polymer-modified media, such as XL and Capto, on the other hand, it is an available binding volume that is generally the strongest determinant of static capacity. Additionally, though, if the resin charge density is low, as it is for Capto, or the protein charge density is high, it seems that the condition of electroneutrality can play a part in determining the maximum adsorption. The semiquantitative analyses in this study should aid in understanding the limiting factors in adsorption, helping to rationally choose solution conditions to maximize adsorption. Of course, achieving a high static capacity is not always the end goal in screening solution conditions, as transport effects are typically very important in column operation, so the adsorption knowledge gained here must be used in tandem with relevant uptake information.

Acknowledgments

We would like to thank DMV-International for donating the lactoferrin and Biogen Idee for donating the mAb. We would also like to thank Shannon Modla of the Delaware Biotechnology Institute for help with TEM imaging. We are grateful for financial support from the NSF (NSF IGERT program and grant CBET-0828590) and the NIH (grant R01 GM75047).

References

1. Müller W. Eur J Biochem 1986;155:213. [PubMed: 2419132]
2. Müller W. J Chromatogr 1990;510:133.
3. Janzen R, Unger KK, Müller W, Hearn MTW. J Chromatogr 1990;522:77.
4. Hearn MTW, Hodder AN, Fang FW, Aguilar MI. J Chromatogr 1991;548:117.
5. Fang FW, Aguilar MI, Hearn MTW. J Chromatogr 1992;599:163.
6. Xie JR, Aguilar MI, Hearn MTW. J Chromatogr A 1995;691:263. [PubMed: 7894652]
7. Xie JR, Aguilar MI, Hearn MTW. J Chromatogr A 1995;711:43.
8. Fang FW, Aguilar MI, Hearn MTW. J Chromatogr A 1996;729:67.
9. Fang FW, Aguilar MI, Hearn MTW. J Chromatogr A 1996;729:49. [PubMed: 9004964]
10. Kaufmann M. J Chromatogr B 1997;699:347.
11. Tsuneda S, Shinano H, Saito K, Furusaki S, Sugo T. Biotechnol Progr 1994;10:76.
12. Tsuneda S, Saito K, Furusaki S, Sugo T. J Chromatogr A 1995;689:211.
13. Tsuneda S, Saito K, Sugo T, Mackuuchi K. Rad Phys Chem 1995;46:239.
14. Matoba S, Tsuneda S, Saito K, Sugo T. Nat Biotechnol 1995;13:795.
15. Camperi SA, del Canizo AAN, Wolman FJ, Smolko EE, Cascone O, Grasselli R. Biotechnol Progr 1999;15:500.
16. Savina IN, Mattiasson B, Galaev IY. Polymer 2005;46:9596.
17. Savina IN, Galaev IY, Mattiasson B. J Mol Recognit 2006;19:313. [PubMed: 16703569]
18. Müller E. Chem Eng Technol 2005;28:1295.
19. Boschetti, E.; Coffman, JL. Bioseparation and Bioprocessing. Wiley-VCH; New York, NY: 1998. p. 157
20. Weaver LE, Carta G. Biotechnol Prog 1996;12:342.
21. Fernandez MA, Carta G. J Chromatogr A 1996;746:169.
22. Fernandez MA, Laughinghouse WS, Carta G. J Chromatogr A 1996;746:185.
23. Lewus RK, Altan FH, Carta G. Ind Eng Chem Res 1998;37:1079.
24. Staby A, Jensen IH. J Chromatogr A 2001;908:149. [PubMed: 11218117]
25. Staby A, Sand MB, Hansen RG, Jacobsen JH, Andersen LA, Gerstenberg M, Bruus UK, Jensen IH. J Chromatogr A 2004;1034:85. [PubMed: 15116917]

26. Ljunglöf A, Thömmes J. J Chromatogr A 1998;813:387. [PubMed: 9700931]
27. Hubbuch J, Linden T, Knieps E, Ljunglöf A, Thömmes J, Kula MR. J Chromatogr A 2003;1021:93. [PubMed: 14735978]
28. Hubbuch R, Linden T, Knieps E, Thömmes J, Kula MR. J Chromatogr A 2003;1021:105. [PubMed: 14735979]
29. Ljunglöf A, Lacki KM, Mueller J, Harinarayan C, van Reis R, Fahrner R, Van Alstine JM. Biotechnol Bioeng 2007;96:515. [PubMed: 17096387]
30. Tugcu N, Roush DJ, Göklen KE. Biotechnol Bioeng 2008;99:599. [PubMed: 17680666]
31. Stone MC, Carta G. J Chromatogr A 2007;1146:202. [PubMed: 17336312]
32. Sophianopoulos AJ, Holcomb DN, Van Holde KE, Rhodes CK. J Biol Chem 1962;237:1107. [PubMed: 13915231]
33. Groves ML. J Am Chem Soc 1960;82:3345.
34. Lewus RA, Sandler SI, Lenhoff AM. 2008in preparation
35. DePhillips P, Lagerlund I, Farenmark J, Lenhoff AM. Anal Chem 2004;76:5816. [PubMed: 15456302]
36. Greenkorn, RA. Flow Phenomena in Porous Media. Marcel Dekker, Inc; New York: 1983.
37. Kronman MJ, Andreotti RE. Biochemistry 1964;3:1145. [PubMed: 14220681]
38. Hayat, MA. Principles and Techniques of Electron Microscopy: Biological Applications. CRC Press; Boca Raton, FL: 1989.
39. Dziennik, SR. Ph.D. dissertation. Department of Chemical Engineering, University of Delaware; Newark, DE: 2002.
40. Dziennik SR, Belcher EB, Barker GA, DeBergalis MJ, Fernandez SE, Lenhoff AM. Proc Natl Acad Sci USA 2003;100:420. [PubMed: 12522150]
41. Lu JR, Su TJ, Howlin BJ. J Phys Chem B 1999;103:5903.
42. DePhillips P, Lenhoff AM. J Chromatogr A 2001;933:57. [PubMed: 11758747]
43. Boardman NK, Partridge SM. Biochem J 1955;59:543. [PubMed: 14363145]
44. Ståhlberg J, Jönsson B, Horváth C. Anal Chem 1991;63:1867. [PubMed: 1789444]
45. DePhillips P, Lagerlund I, Farenmark J, Lenhoff AM. Anal Chem 2004;76:5816. [PubMed: 15456302]
46. Xu X, Lenhoff AM. J Phys Chem B 2008;112:1028. [PubMed: 18171041]
47. Haggerty L, Sugarman JH, Prudhomme RK. Polymer 1988;29:1058.
48. Roth, D.; Daniels, C.; To, B. Poster BIOT-318 presented at 234th ACS National Meeting; Boston. 2007.
49. Dziennik SR, Belcher EB, Barker GA, Lenhoff AM. Biotechnol Bioeng 2005;91:139. [PubMed: 15889407]
50. Harinarayan C, Mueller J, Ljunglöf A, Fahrner R, Van Alstine J, van Reis R. Biotechnol Bioeng 2006;95:775. [PubMed: 16897740]
51. DePhillips P, Lenhoff AM. J Chromatogr A 2000;883:39. [PubMed: 10910199]
52. Yao Y, Lenhoff AM. J Chromatogr A 2006;1126:107. [PubMed: 16844131]
53. Brooks CA, Cramer SM. AIChE J 1992;38:1969.
54. Tanemura M. Ann Inst Stat Math 1979;31:351.
55. Feder J. J Theor Biol 1980;87:237.
56. Hinrichsen EL, Feder J, Jossang T. J Stat Phys 1986;44:793.
57. Dickman R, Wang JS, Jensen I. J Chem Phys 1991;94:8252.
58. Ogston AG. Trans Faraday Soc 1958;54:1754.
59. Laurent TC, Killander J. J Chromatogr 1964;14:317.
60. Russel, WB.; Saville, DA.; Schowalter, WR. Colloidal Dispersions. Cambridge University Press; Cambridge, UK: 1989.
61. Snoussi K, Halle B. Biophys J 2005;88:2855. [PubMed: 15665132]
62. Sharma U, Carbeck JD. Electrophoresis 2005;26:2086. [PubMed: 15861469]
63. Bowen WR, Cao XW, Williams PM. Proc R Soc London, Ser A 1999;455:2933.

64. Hartmann WK, Saptharishi N, Yang XY, Mitra G, Soman G. Anal Biochem 2004;325:227. [PubMed: 14751257]
65. Tanford C, Roxby R. Biochemistry 1972;11:2192. [PubMed: 5027621]
66. Dolinsky TJ, Nielsen JE, McCammon JA, Baker NA. Nucleic Acids Res 2004;32:W665. [PubMed: 15215472]
67. Li H, Robertson AD, Jensen JH. Proteins 2005;61:704. [PubMed: 16231289]
68. Dismer F, Petzold M, Hubbuch J. J Chromatogr A 2008;1194:11. [PubMed: 18234205]
69. Ye XY, Wang HX, Liu F, Ng TB. Int J Biochem Cell Biol 2000;32:235. [PubMed: 10687957]
70. Wetter LR, Deutsch HF. J Biol Chem 1951;192:237. [PubMed: 14917670]
71. Plate K, Beutel S, Buccholz H, Demmer W, Fischer-Fruhholz S, Reif O, Ulber R, Scheper T. J Chromatogr A 2006;1117:81. [PubMed: 16616760]
72. Canfield R. J Biol Chem 1963;238:2698. [PubMed: 14063294]
73. Moore S, Anderson B, Groom C, Haridas M, Baker E. J Mol Biol 1997;274:222. [PubMed: 9398529]
74. Ahamed T, Esteban BNA, Ottens M, van Dedem GWK, van der Wielen LAM, Bisschops MAT, Lee A, Pham C, Thömmes J. Biophys J 2007;93:610. [PubMed: 17449660]
75. Krivanek R, Rybar P, Küpcü S, Sleytr UB, Hianik T. Bioelectrochem 2002;55:57.
76. Baker NA, Sept D, Joseph S, Holst MJ, McCammon JA. Proc Natl Acad Sci USA 2001;98:10037. [PubMed: 11517324]

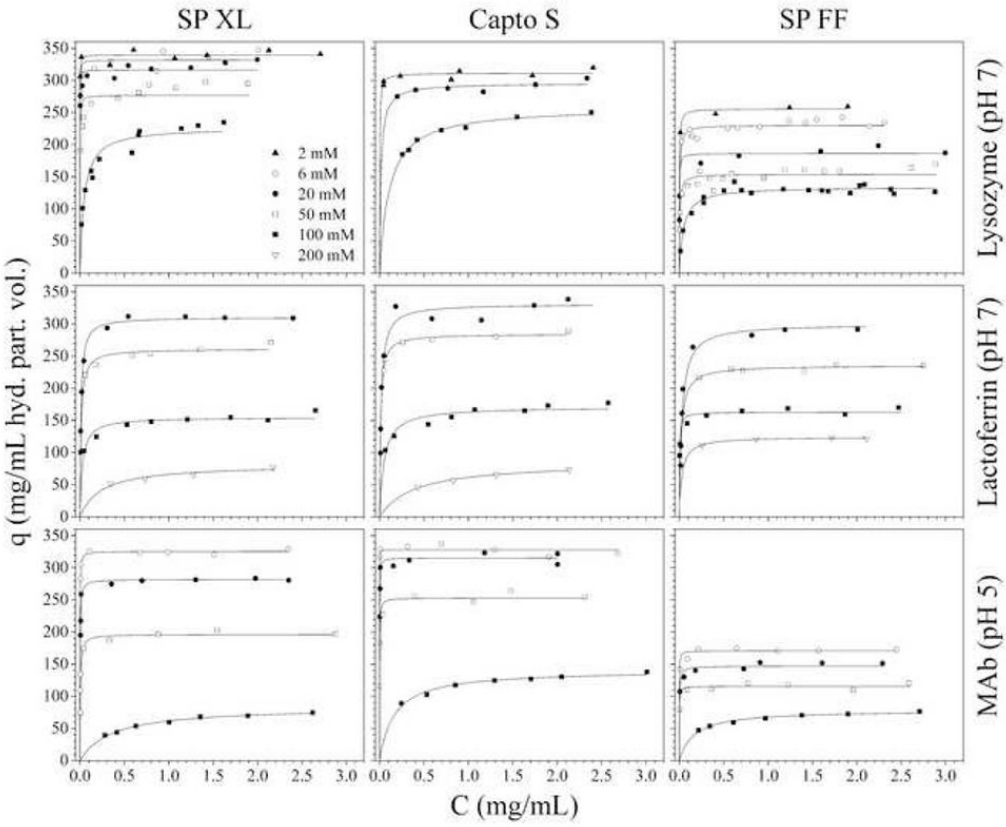

Figure 1.
Adsorption isotherms for the indicated protein-resin pairings. The pH is specified for each protein and total ionic strengths are shown in the top left panel.

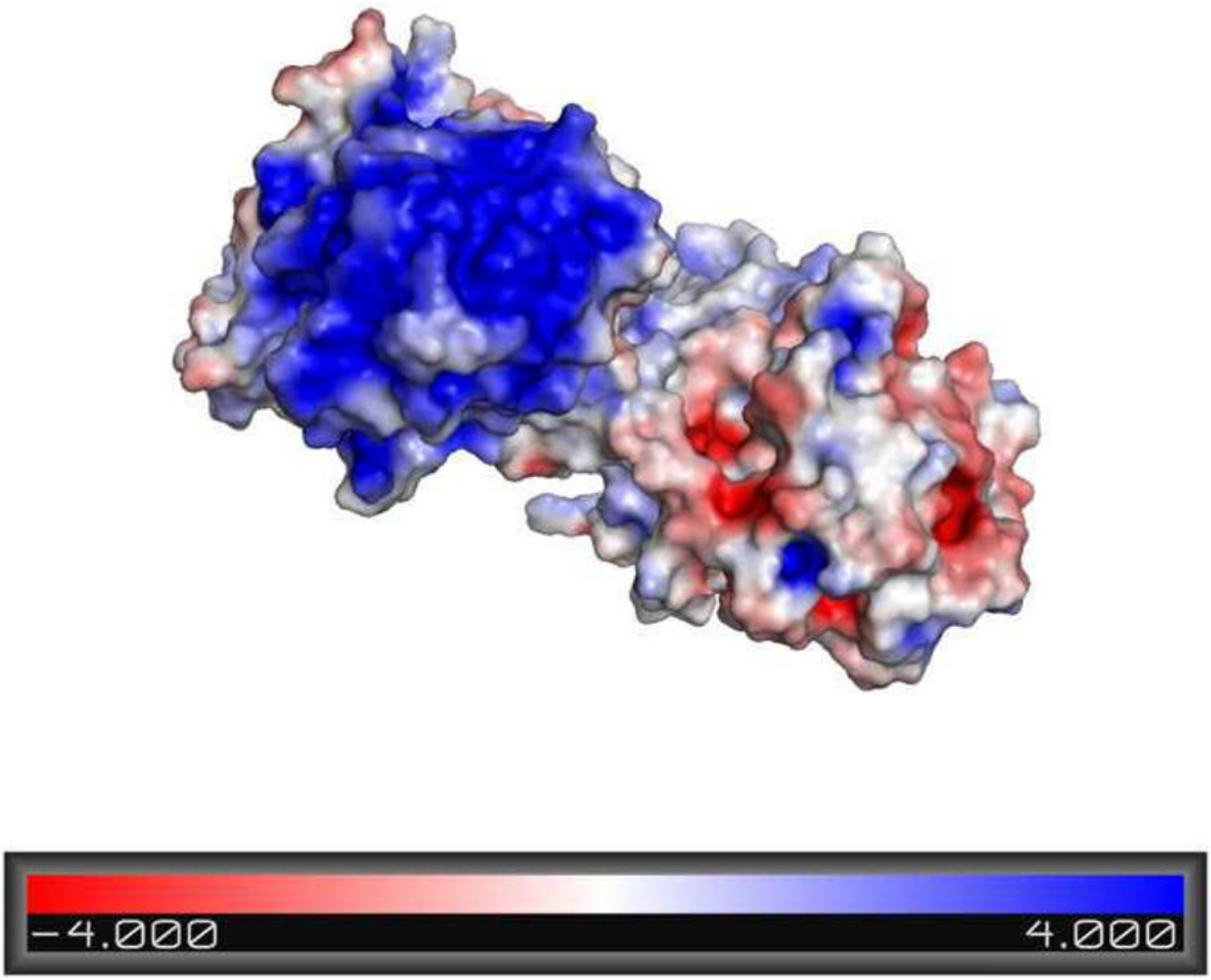

Figure 2.
Surface potential map of pH 7 lactoferrin. The scale bar is in units of kT/e = 0.025 V at 22°C. The patch visible on the left lobe of the protein can be seen to be very positively charged with the rest of the molecule being relatively neutral by comparison. The image was generated in PyMOL and required use of the PDB2PQR [66], PropKa [67], and APBS [76] software.

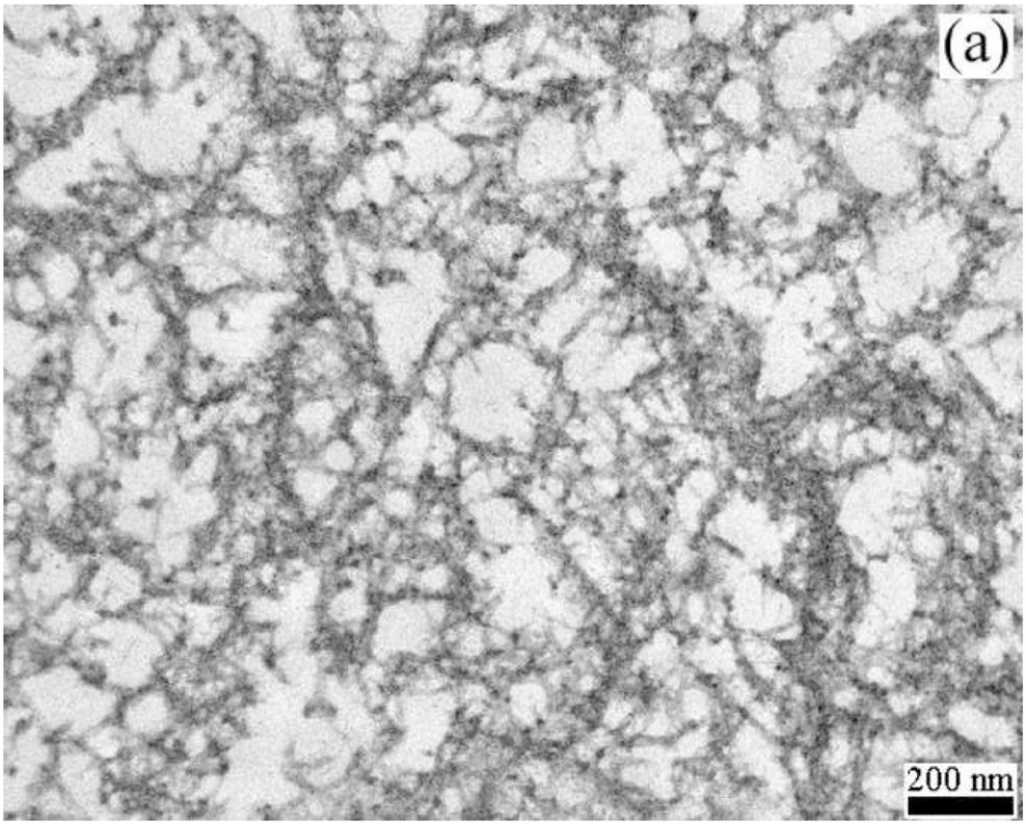

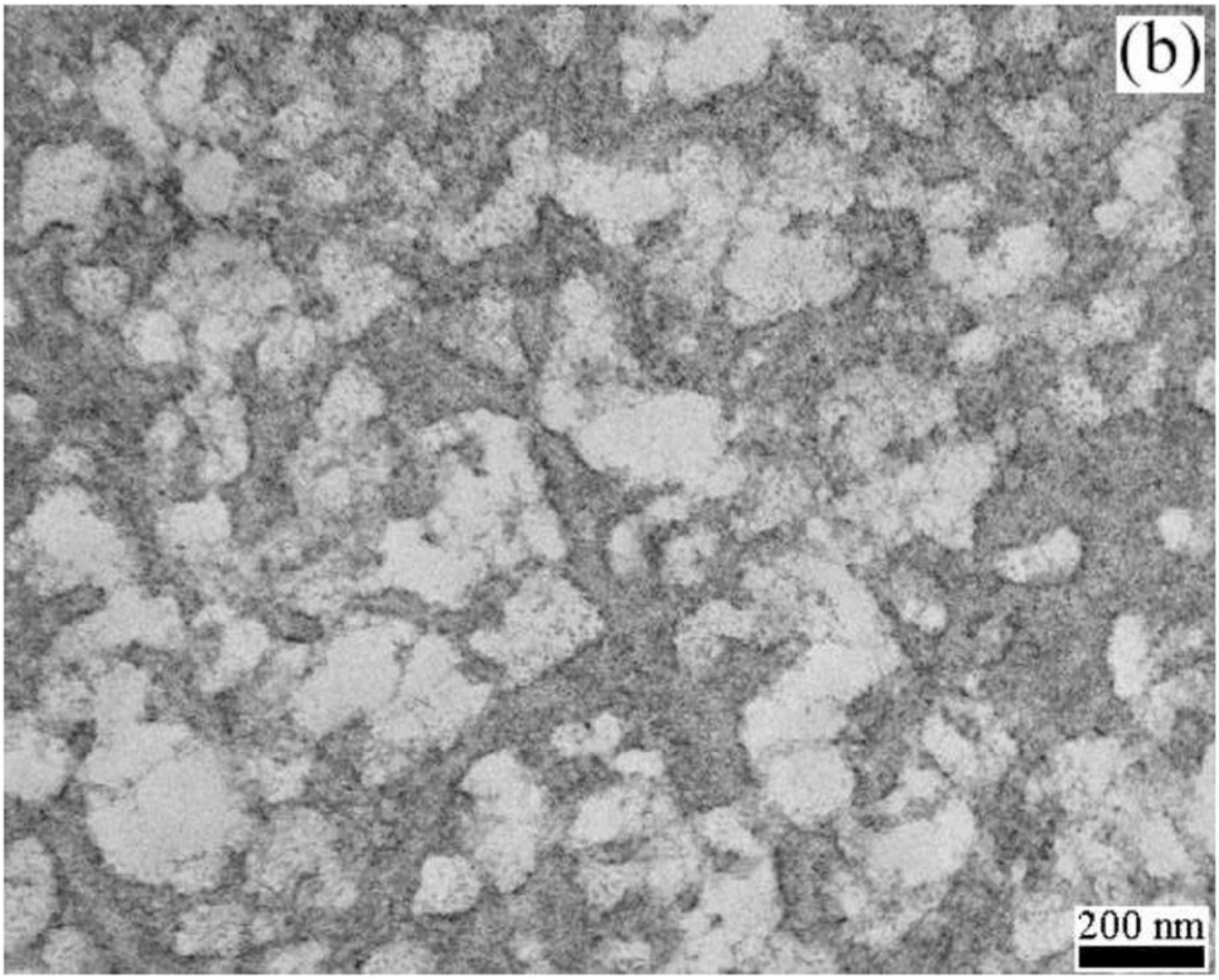

Figure 3.
TEM images for low adsorbed protein concentrations, (a) Q Sepharose FF. (b) Q Sepharose XL.

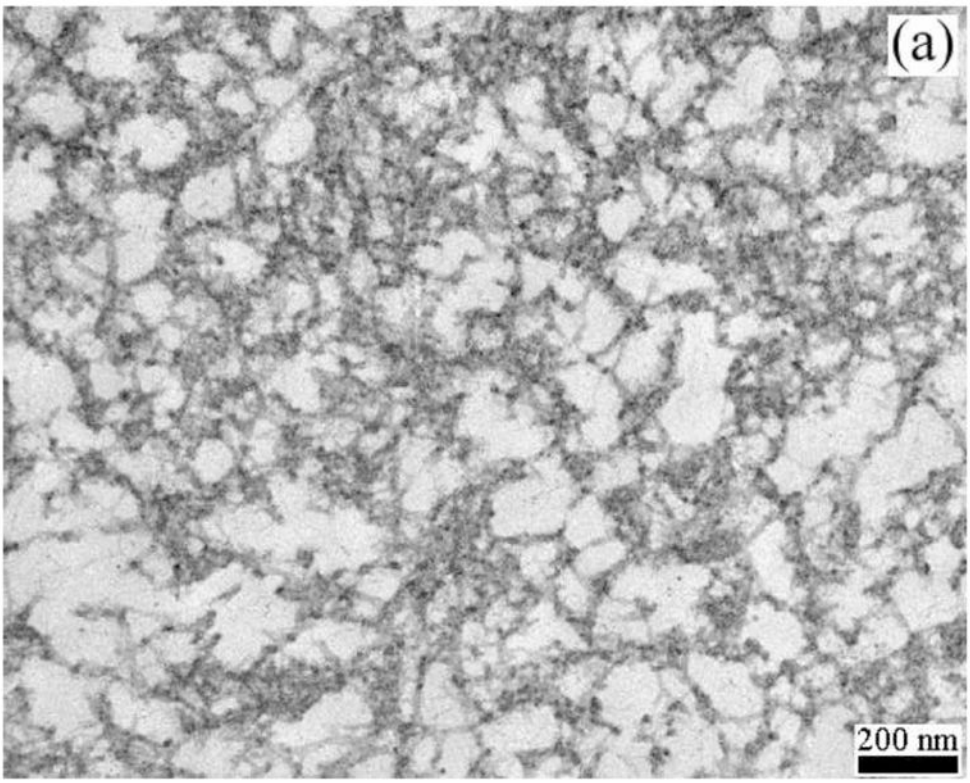

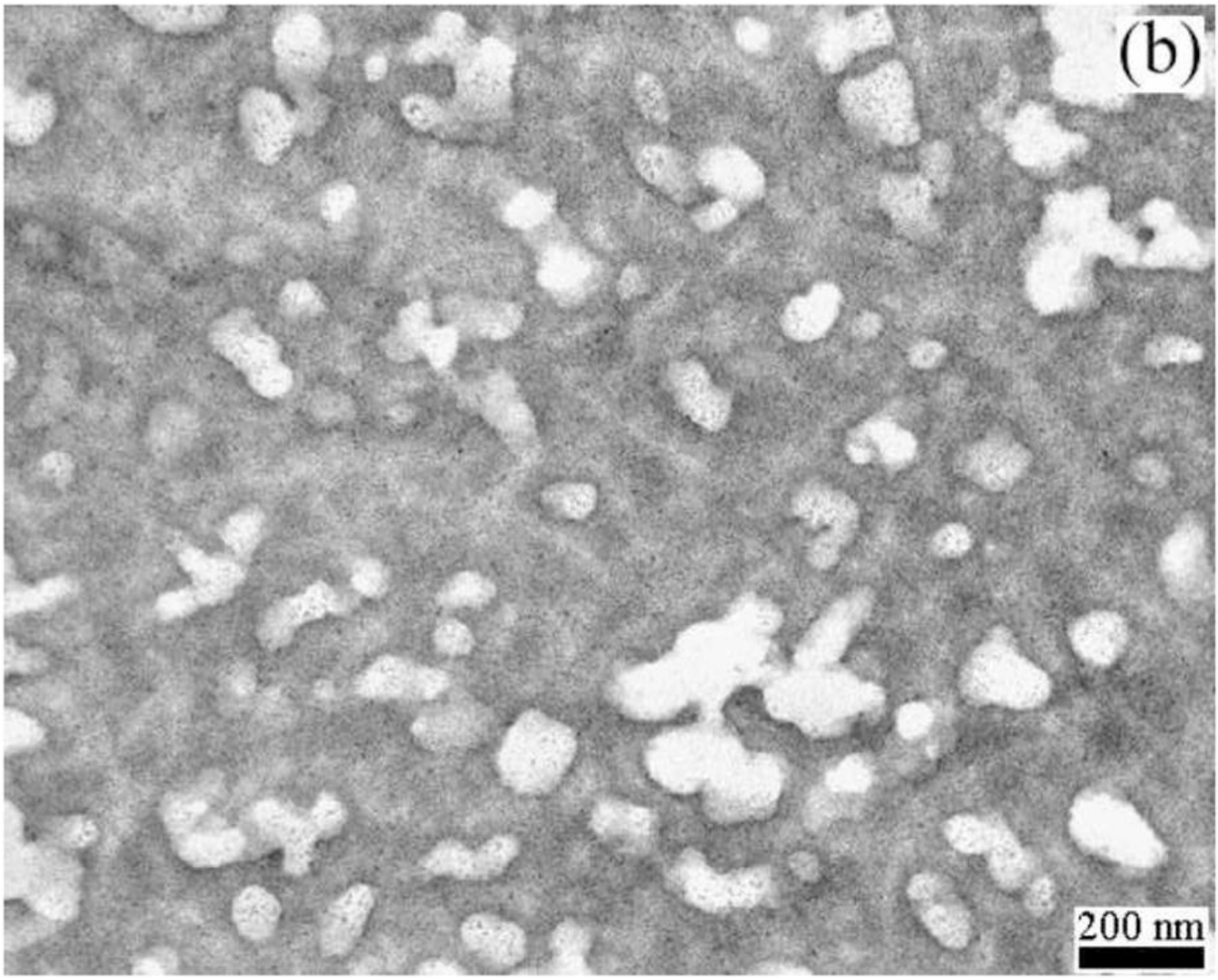

Figure 4.
TEM images for high adsorbed protein concentrations, (a) Q Sepharose FF. (b) Q Sepharose XL.

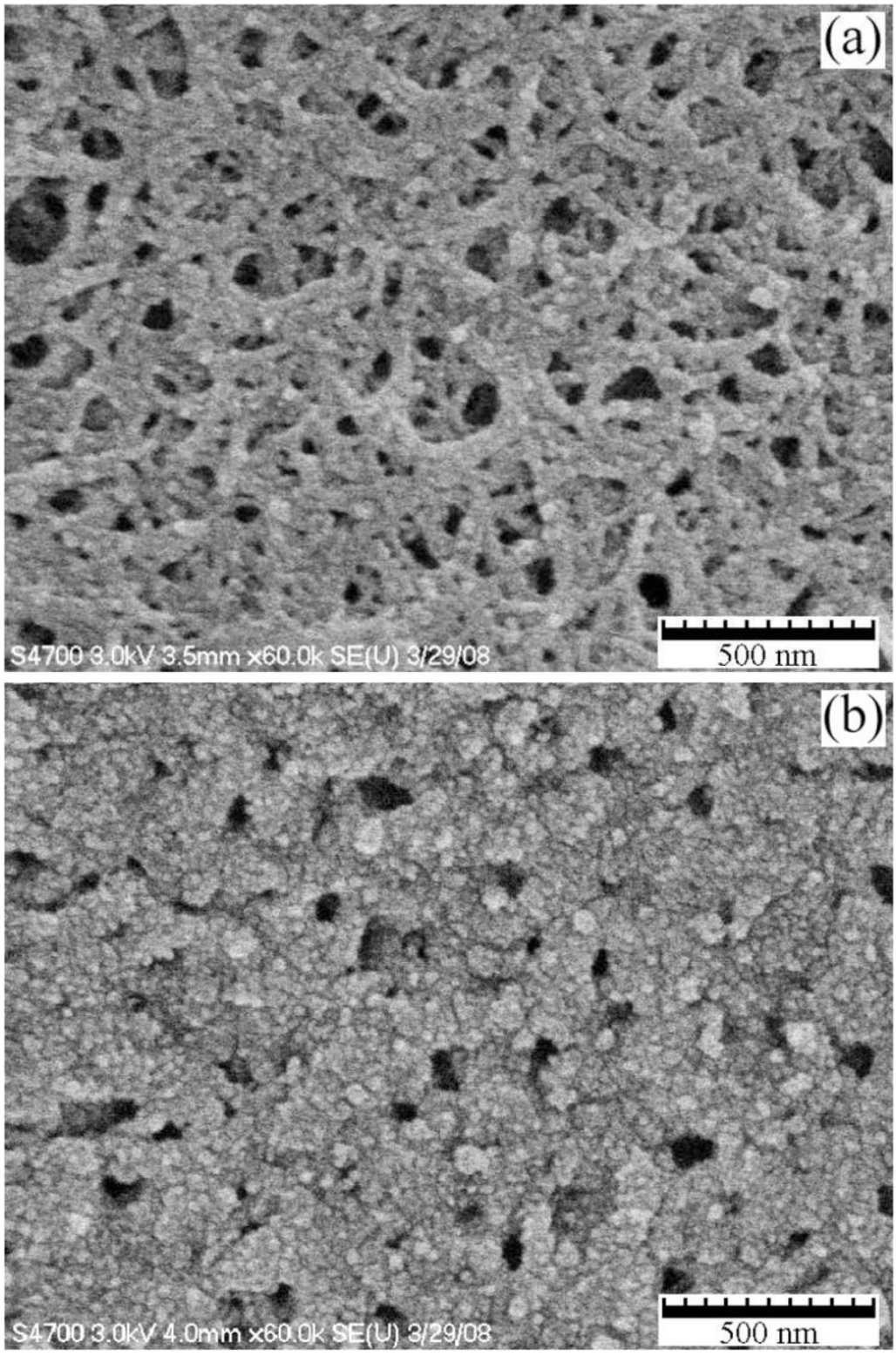

Figure 5.
SEM images for high adsorbed protein concentrations. (a) Q Sepharose FF. (b) Q Sepharose XL.

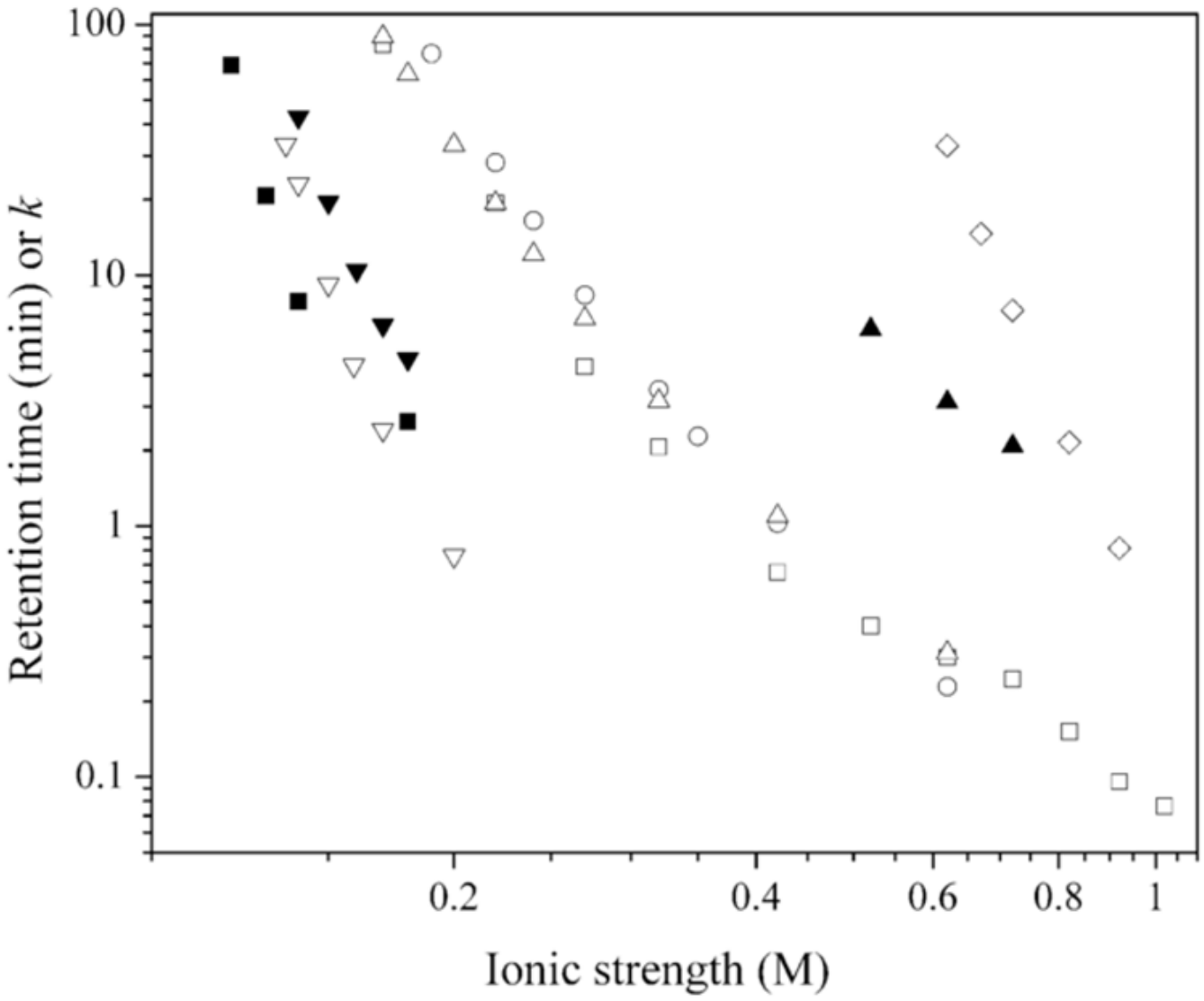

Figure 6.
Isocratic retention data for the studied protein-resin pairings. Experiments are at pH 7 for lysozyme and lactoferrin and at pH 5 for the mAb. Open symbols indicate *k* values: mAb on SP FF (▽); lysozyme on SP FF (□), Capto S (△), and SP XL (○); lactoferrin on SP FF (◇). Closed symbols indicate retention times: mAb on SP XL (■) and Capto S (▼;), lactoferrin on SP XL (▲). Note that the retention times are single data points while the points for *k* were run in triplicate.

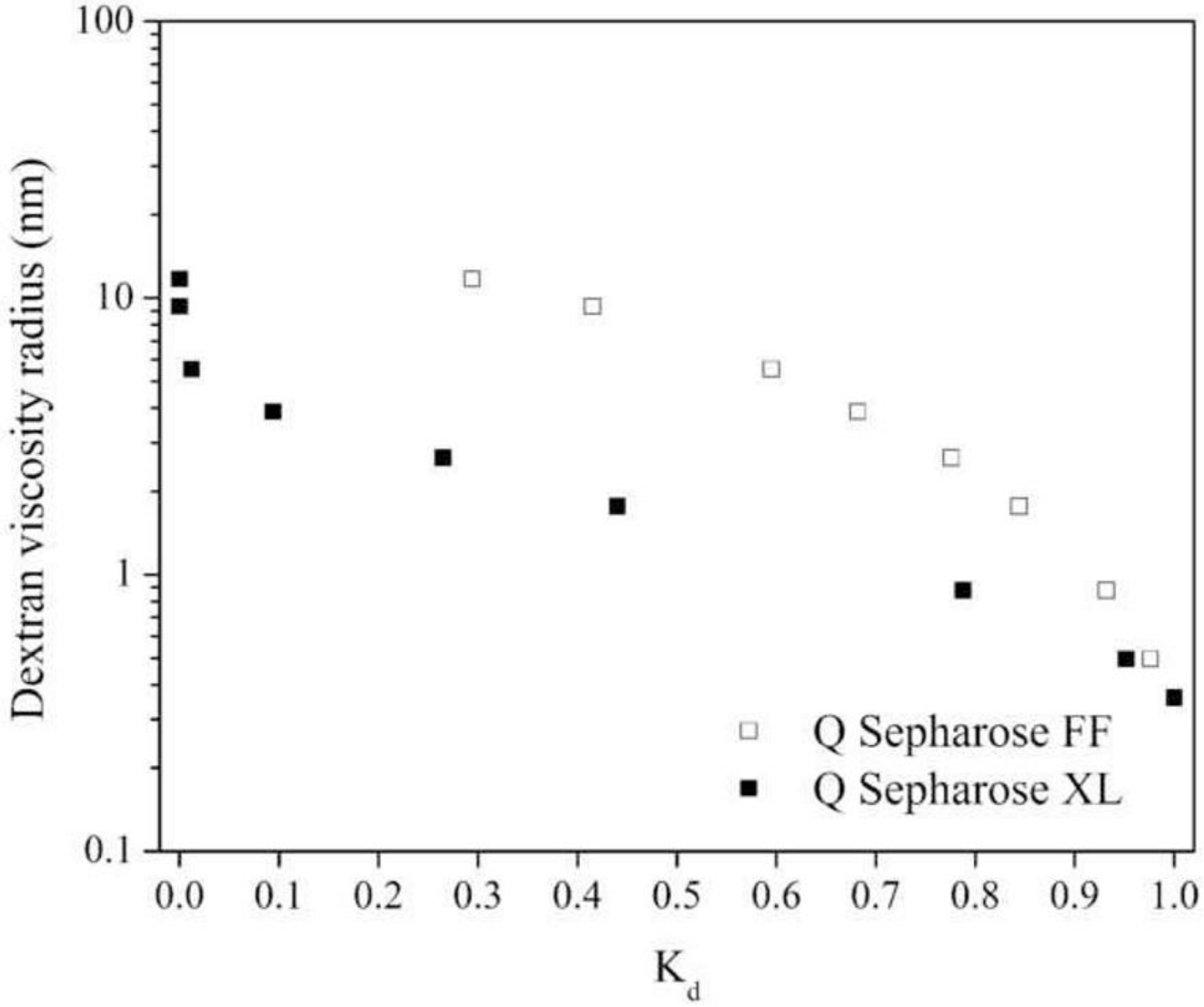

Figure 7.
Inverse SEC distribution coefficients as a function of probe size [52].

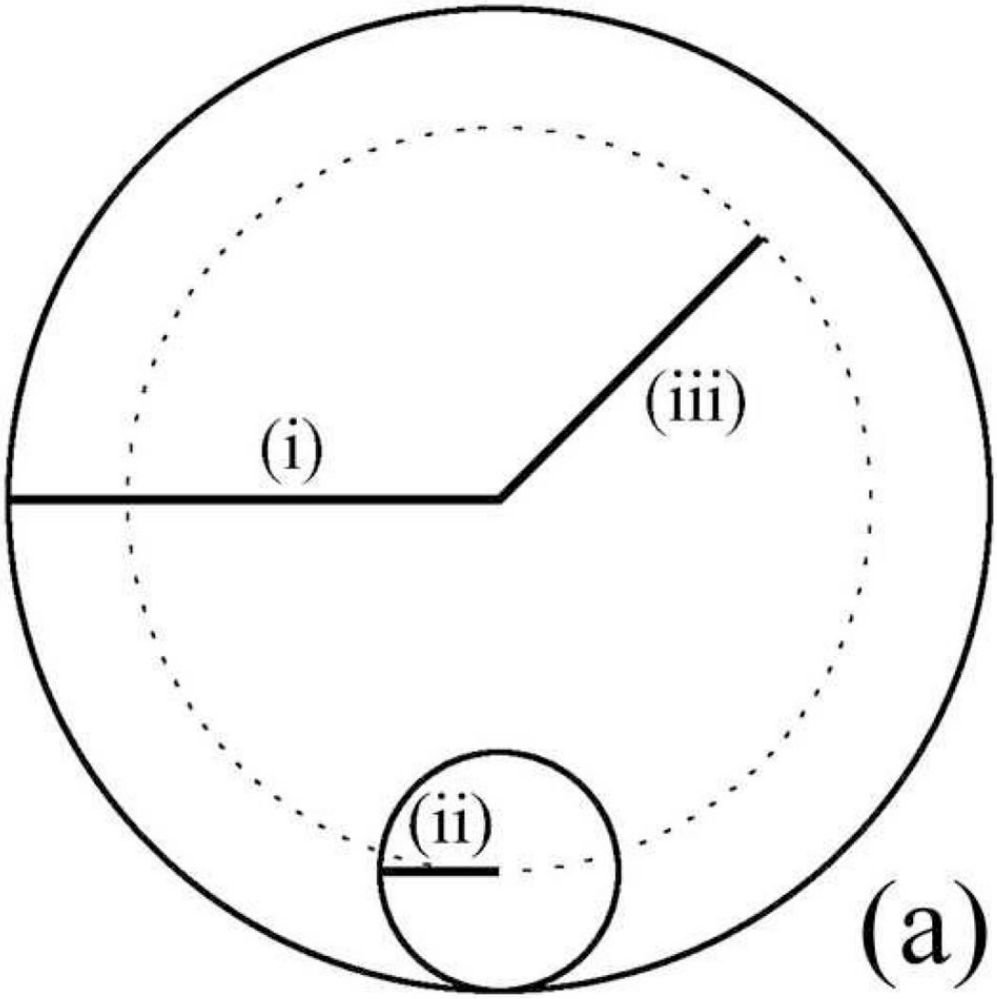

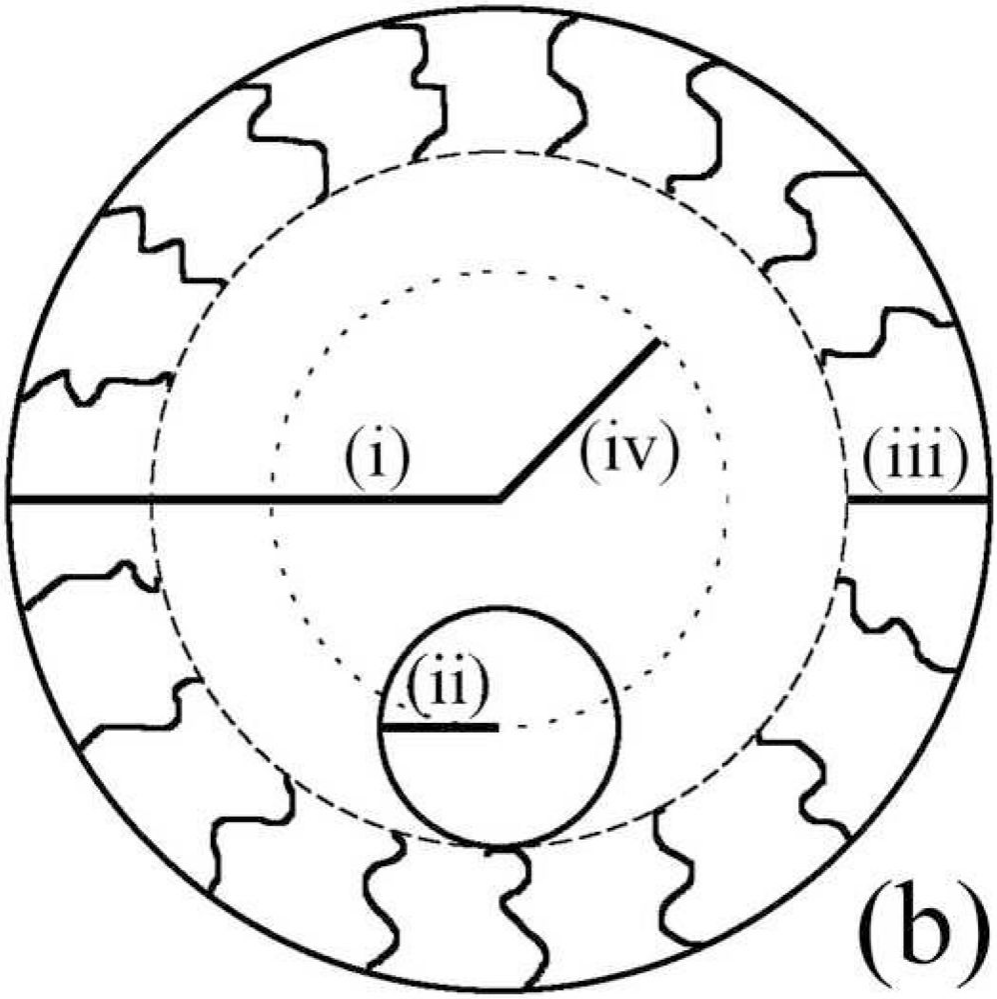

Figure 8.

Pore cross sections for idealized cylindrical pores, (a) FF-type pore with relevant radii (i) R_{pore}, (ii)r_{porbee}, (iii) $(R_{pare} - r_{probe})$. (b) XL-type pore with relevant radii (i) R_{pore}, (ii) r_{porbee}, (iii) r_{dex}, (iv) $(R_{pare} - r_{probe} - r_{dex})$. Note that, for simplicity, the multi-point attachment of the dextran has not been depicted.

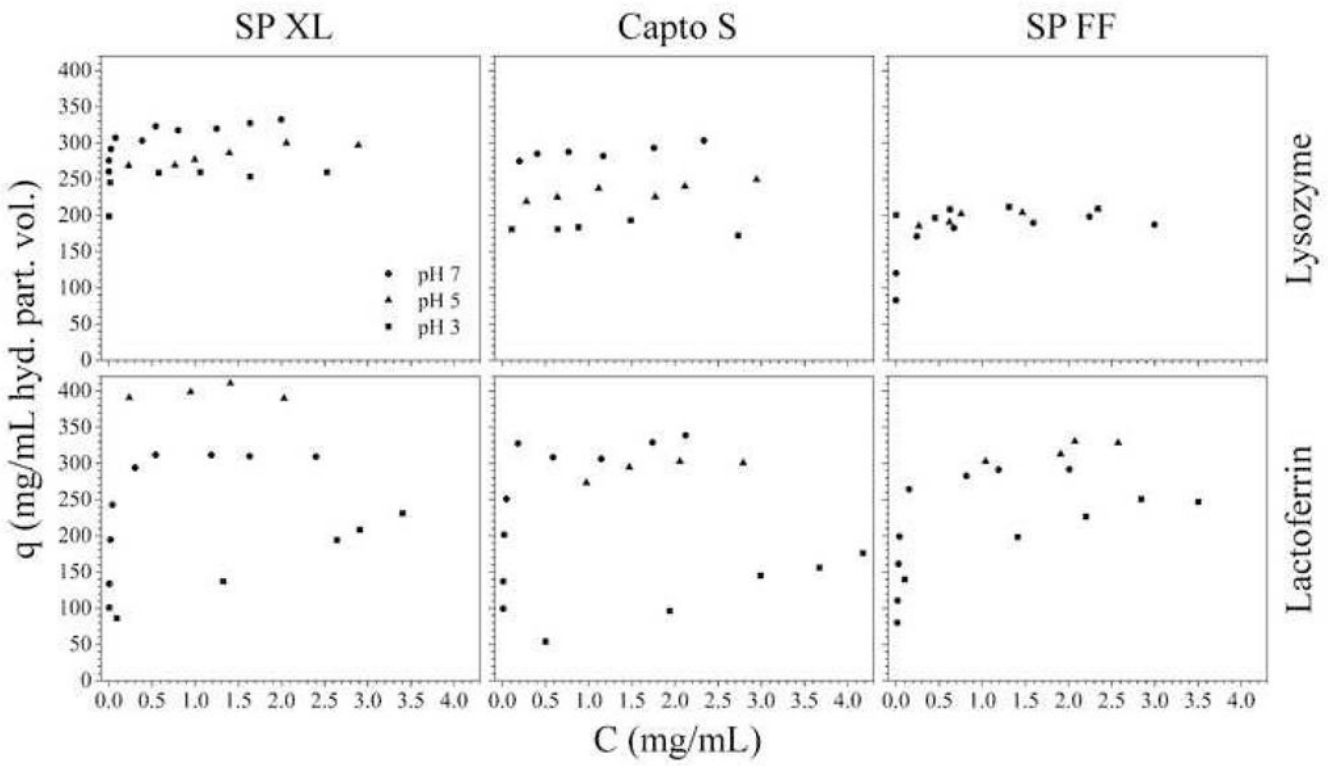

Figure 9.
Adsorption isotherms for the indicated protein-resin pairings at 20 mM TIS. The pH values are specified in the top left panel.

Table 1

Relevant protein properties.

Property	Lysozyme	Lactoferrin	MAb
PI	11.4 [70]	8.8 [71]	≈8
M_w (kDa)	14.3 [72]	78 [73]	144 [74]
Partial specific volume (mL/g)	0.703 [32]	0.725 [33]	0.7 [75,74]
Radius (nm)[a]	1.6	2.8	3.4

[a] Radius of sphere of equivalent volume.

Table 2

Physical properties of the stationary phases as determined by the manufacturer.

Resin	Base matrix	Functional group	Particle size range, mean (μm)	Ion capacity (μmol/mL)
SPFF	agarose	sulfonate on 6-carbon spacer	45–165, 90	180–250
SPXL	agarose with dextran extenders	sulfonate on 6-carbon spacer	45–165, 90	180–250
Capto S	high flow agarose with dextran extenders	sulfonate on 2-carbon spacer	NA, 90	110–140

Table 3

Estimated maximum static capacities (mg/mL hydrated resin volume) at pH values studied. Low and high refer to balances based on the low and high resin charge densities. Net charges for lysozyme [65] and lactoferrin [66,67] are listed at each pH.

	Resin	pH7 Low	pH7 High	pH5 Low	pH5 High	pH3 Low	pH3 High
Lysozyme							
Net charge		+8		+10		+15	
	SP FF	550	760	440	610	290	410
	SP XL	520	720	410	570	280	380
	Capto S	330	420	260	330	170	220
Lactoferrin							
Net charge		+16		+24		+78	
	SP FF	1500	2080	1000	1390	310	430
	SP XL	1410	1960	940	1310	290	400
	Capto S	890	1140	600	760	180	230